

# SODIUM METAL BATTERY USING COBALTOXIDE THROUGH IN SITU PLATING OF SODIUM METAL

Saurav L. Chaudhari,<sup>†</sup> Ketan P. Pise<sup>‡</sup> 

<sup>†</sup>

Department of Electronics Engineering, Shri Sant Gajanan Maharaj College of Engineering, Shegaon 444203, India

<sup>‡</sup>

Department of IT, Shri Sant Gajanan Maharaj of Engineering, Shegaon 444203, India

\* Supporting Information

**ABSTRACT:** In this work, we demonstrate that an impugn of energy density for sodium chemistries can be prevail through an anode-free architecture enabled by the use of a (nanocarbon/Cobaltoxide) nucleation layer formed on Aluminium current collectors. Electrochemical studies show this configuration to provide highly stable and efficient plating and stripping of sodium metal over a range of currents up to 5 mA/cm<sup>2</sup>, sodium loading up to 14 mAh/cm<sup>2</sup>, and with long-term endurance exceeding 1000 cycles at a current of 0.7 mA/cm<sup>2</sup>. Building upon this anode-free architecture, we demonstrate a full cell using a presodiated pyrite cathode to achieve energy densities of ~400 Wh/kg, far surpassing recent reports on SIBs and even the theoretical maximum for LIB technology while still relying on naturally abundant raw materials and cost-effective aqueous processing

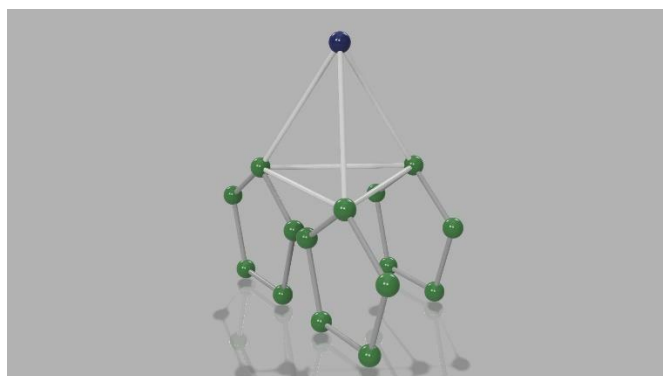
**KEYWORDS:** Metal anode, iron pyrite, sodium battery, current collector, energy density, anode-free

Here, we have taken a huge reference from research paper:

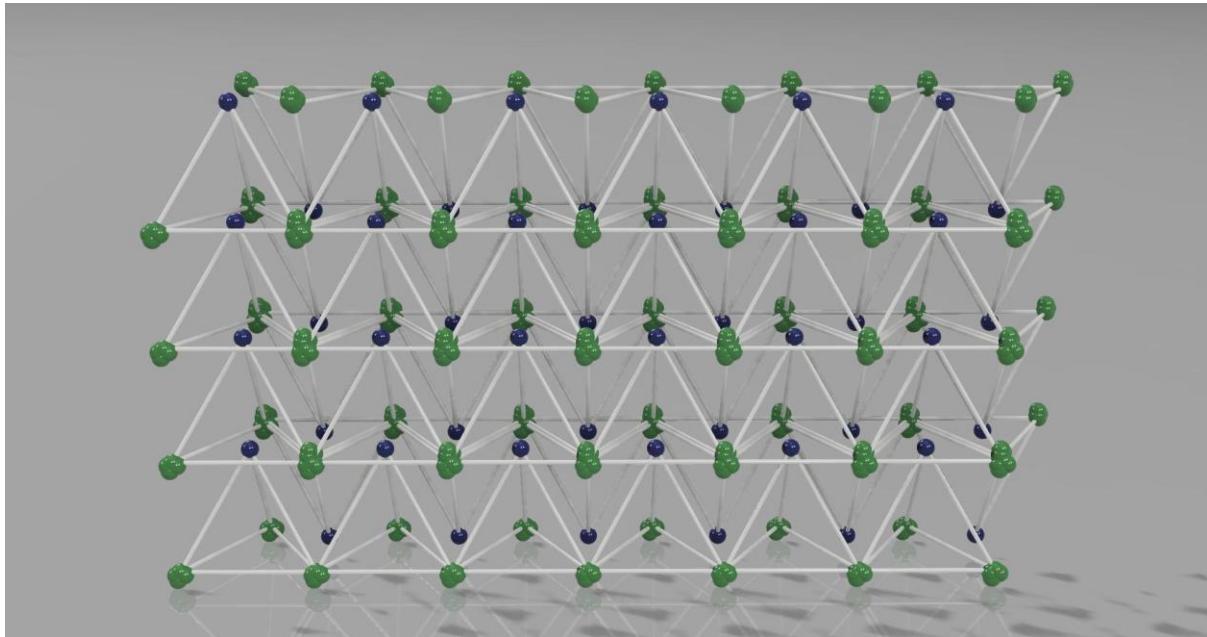
[Anode-Free Sodium Battery through in Situ Plating of Sodium Metal](#)

**But have made few additions as follows:**

We have replaced the standard Na<sub>15</sub>Sn<sub>4</sub> with our proposed structured Na<sub>15</sub>Sn<sub>4</sub> which looks like,



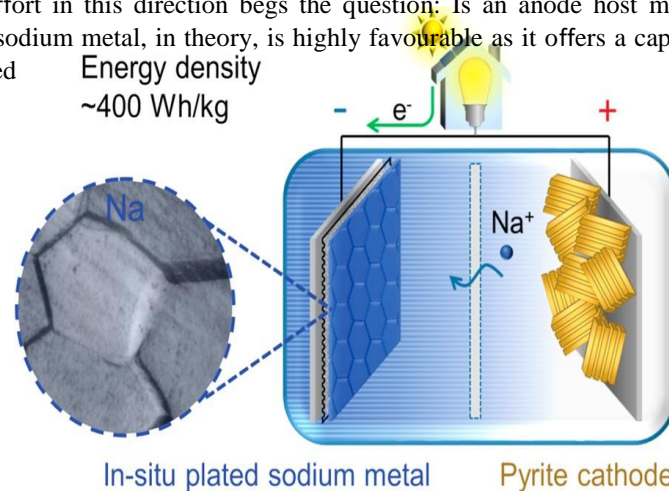
Where the pyramid is made up of Sn atoms and the pentagons are made up of Sodium atoms, its chain structure looks like this



To enable the utilization of our rapidly growing capacity of renewable resources and avoid the curtailment of renewable energy generation without sacrificing grid reliability, batteries are necessary to modernize our electricity grid. Sodium ion batteries (SIBs) have emerged as the most direct route to developing more cost-effective and more sustainably produced metal-ion batteries due to their similarity in chemistry to LIBs and the 1000× greater natural abundance of sodium in comparison to lithium.<sup>1,2</sup>

The pursuit of a SIB design suitable for commercialization has spurred a recent surge in research activity focused on developing electrodes capable of hosting sodium ions. However, the larger ionic radius and less negative standard reduction potential (in comparison to lithium ions) have limited the energy density of emerging SIB technology, with recent state-of-the-art full cells demonstrating only ~200 Wh/kg with respect to active mass.<sup>2-6</sup> On this front, the anode side has proven to be the most challenging, as graphite, the standard LIB anode, cannot intercalate sufficient sodium ions. While alternative anode materials including disordered carbons<sup>5,7-10</sup> and alloying metals,<sup>4,11</sup> such as Sn, Sb, or Pb, have been extensively researched with notable progress made, a sodium-ion anode that can deliver high capacity and operate at practical currents without sacrificing cycling performance or Coulombic efficiency is yet to be realized.

The continued research effort in this direction begs the question: Is an anode host material truly needed? Transitioning to “host-less” sodium metal, in theory, is highly favourable as it offers a capacity of 1166 mAh/g (more than double the charged



state of the Sn anode:  $\text{Na}_{15}\text{Sn}_4$ ), as well as the lowest achievable redox potential for a sodium anode, which is especially critical in the transition to emerging S and  $\text{O}_2$  cathodes.<sup>12,13</sup> Furthermore, the density of sodium metal ( $0.97 \text{ g/cm}^3$ ) also serves to maximize volumetric capacity and achieve high areal loading, making the common

trade-off between gravimetric and volumetric performance obsolete. Finally, since the plating/ stripping reactions takes place on the surface, there are no solid-state diffusion limitations, and as a result, extremely high rate capabilities are possible without relying on high-surface area electrodes

Despite these clear advantages of a sodium metal battery, research on room-temperature sodium metal electrodes is emergent and currently remains sparse. In 2015, it was shown that sodium metal is less stable with carbonate electrolytes than lithium metal, due to the organic solid–electrolyte interface (SEI) formed.<sup>14</sup> More recently, there have been initial reports on controlling this SEI layer, either through the use of alternative electrolytes, notably NaPF<sub>6</sub> in glyme<sup>15</sup> or highly concentrated NaFSI in glyme,<sup>16</sup> to form more stable inorganic SEI layers or by directly depositing an artificial inorganic SEI layer on sodium metal electrodes.<sup>17</sup> However, there has been no research addressing the accompanying issues associated with (1) the interface between the sodium metal and the current

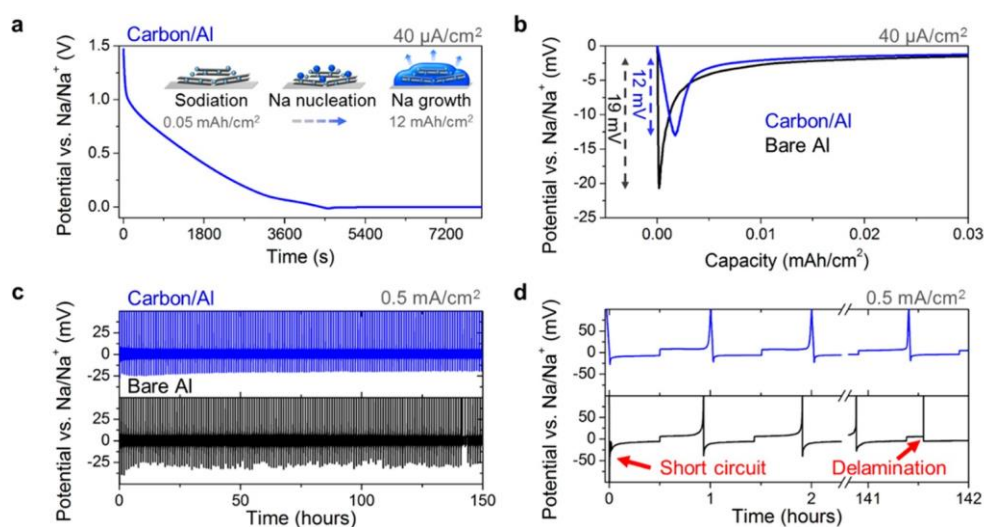


Figure 1. (a) Galvanostatic sodiation and then plating for carbon/Al current collector at  $40 \mu\text{A}/\text{cm}^2$  with carbon loading of  $400 \mu\text{g}/\text{cm}^2$ . (b) Comparison of the sodium nucleation overpotential for bare Al and carbon/Al current collectors at  $40 \mu\text{A}/\text{cm}^2$ . (c) Cycling of bare Al and carbon/Al current collectors at  $0.5 \text{ mA}/\text{cm}^2$  with 30 min plating times with (d) enlarged voltage profiles.

collector, (2) the uneven deposition of sodium on the current collector, or (3) the large volumetric expansion during deposition, which, in addition to engineering the SEI, have all been identified as critical in recent research on current collectors for lithium metal batteries<sup>18–28</sup> and are essential for developing an anode-free sodium metal battery.

In this Letter, we demonstrate a new approach that allows us to overcome both capacity and cycling limitations faced by sodium-ion anodes by abandoning the anode host and, instead, plating sodium metal in situ on an Al current collector equipped with a nucleation layer. In this design, the nucleation layer functions to both assist the sodium seeding process with a lower nucleation energy barrier and improved structure for stable sodium plating. This is demonstrated by results indicating that over 1000 plating-stripping cycles, an average Coulombic efficiency of 99.8% is maintained with a low average hysteresis of 14 mV and smooth sodium film formation. To construct a full cell sodium battery we showcase this anode-free sodium battery with a presodiated pyrite cathode to provide energy density of  $\sim 400 \text{ Wh}/\text{kg}$ , surpassing current SIB and LIB chemistries while simultaneously relying on earth-abundant raw materials such as carbon, aluminum, and sodium with straightforward aqueous processing.

With the goal of developing a design to enable efficient in situ plating,<sup>29,30</sup> we assembled carbon films on Al foil using conductive carbon black (TIMCAL Super C45) and sodium carboxymethyl cellulose (CMC) with aqueous processing, in line with the recent effort to avoid expensive N-methylpyrrolidone (NMP) processing for battery electrodes.<sup>31</sup> Cathode electrodes were processed in a similar fashion using pyrite (FeS<sub>2</sub>), carbon black, and CMC

on Al foil. An electrolyte of 1 M NaPF<sub>6</sub> in diethylene glycol dimethyl ether (diglyme) was used as the electrolyte due to its stability against sodium metal and tendency to form stable SEI layers for sodium-based chemistries.<sup>4,15,32</sup>

To evaluate the role of the carbon nucleation layer on the sodium plating process, we performed galvanostatic plating at low currents (to minimize diffusion limitations) for both bare Al and carbon/Al substrates. Al was selected instead of Cu because it offers significant cost (~3× cheaper) and weight (~3× lighter) benefits, a great advantage made available by transitioning to sodium-based chemistries. Figure 1a shows the sodiation of the carbon/Al current collector, where the sloping potential curve above 0 V vs Na/Na<sup>+</sup> corresponds to the storage of sodium ions in disordered carbon, and the steady voltage reached below 0 V corresponds to the plating of sodium metal. While this figure highlights the sodiation and initial plating that occurs, it is important to note that the capacity provided by the sodiation of the carbon layer, 0.05 mAh/cm<sup>2</sup> (or 120 mAh/g), is negligible in comparison to the plating capacities, up to 12 mAh/cm<sup>2</sup>, we demonstrate in this work. Subsequent plating and stripping testing was performed below 100 mV, so the carbon nucleation layer remained mostly sodiated throughout these tests. Accordingly, we refer to the carbon/Al electrodes as current collectors for anode-free cells as the meaningful capacity is achieved through the in situ plating of the sodium metal.

Comparing the plating process for a sodiated carbon and a bare Al current collector (Figure 1b), we observe that nucleation overpotential (difference between the bottom of the trough where nucleation occurs and the steady-state plating potential) is reduced from 19 to 12 mV by the carbon layer. Reducing this nucleation barrier is critical for facilitating a smoother deposition, minimizing parasitic reactions, and allowing for high-rate performance. The improved performance observed can be attributed to the increased surface area provided by the carbon (~180× increase in surface area for a 400 μg/cm<sup>2</sup> carbon layer),<sup>22,24,33</sup> the presence of highly reactive sp<sup>3</sup> carbon sites and oxygen-containing functional groups (Figure S1), and the initial storage of sodium ions in the carbon. These observations provide the first examination of the importance of substrate on the nucleation of sodium metal and compliment recent work performed by Yan et al. on the effect of substrate on the nucleation of lithium metal.<sup>26</sup> Going forward, this work motivates the engineering of carbons nanomaterials for facilitating sodium nucleation, bridging the extensive literature aimed at designing carbon materials for sodium ion storage forward to higher energy density sodium metal batteries.

Figure 1c shows 150 h of plating/stripping cycles performed at an increased rate of  $0.5 \text{ mA/cm}^2$ . Examining the initial cycles (shown in Figure 1d), we see that during the first plating process the bare Al electrode exhibits signs

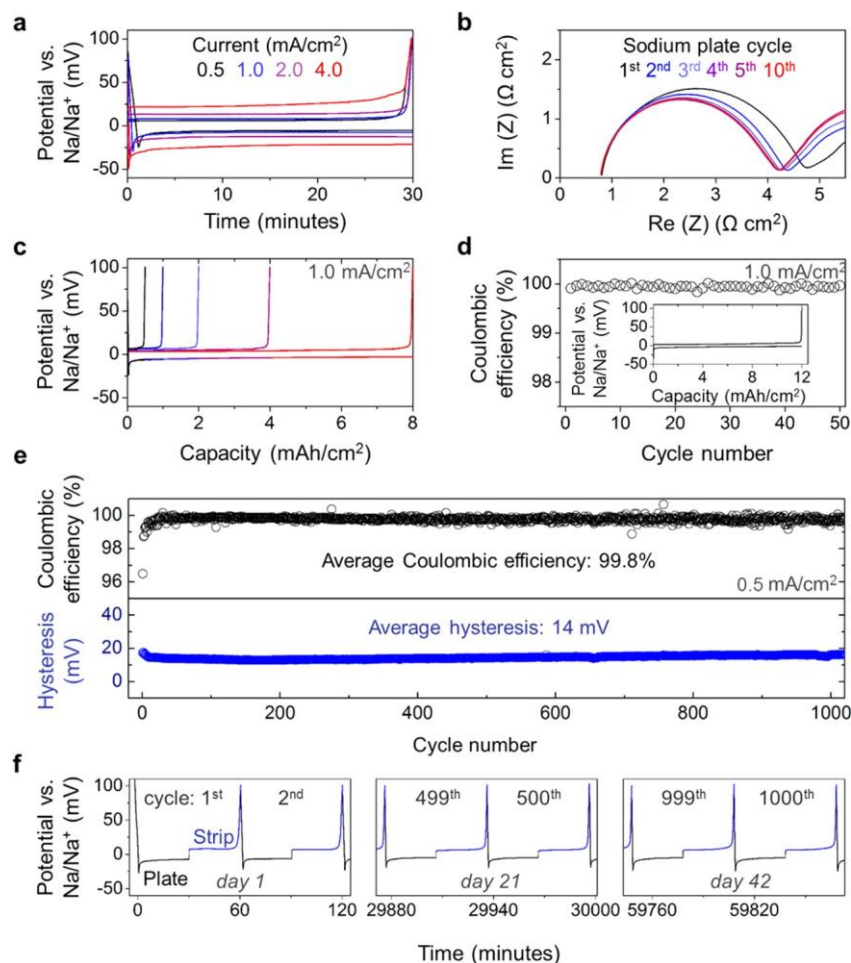


Figure 2. (a) Galvanostatic plating/stripping of sodium on carbon/Al current collectors performed over a range of currents for 30 min plating times. (b) Nyquist curves performed after initial plating cycles with  $0.25 \text{ mAh/cm}^2$  loading. (c) Galvanostatic plating/stripping of sodium on carbon/Al current collectors performed over a range of times (or loadings) at  $1.0 \text{ mA/cm}^2$ . (d) Fifty cycles performed at  $1 \text{ mA/cm}^2$  with  $12 \text{ mAh/cm}^2$  loading of sodium with the inset showing a corresponding potential profile. (e) Coulombic efficiency and voltage hysteresis from over 1000 plating/stripping cycles performed at  $0.5 \text{ mA/cm}^2$  with  $0.25 \text{ mAh/cm}^2$  loading. (f) Corresponding potential profiles of the 1st, 2nd, 499th, 500th, 999th, and 1000th plating/stripping cycles.

of shorting, which we attribute to the uneven plating that occurs due to the higher nucleation overpotential. In contrast, the prone to failure at these currents (Figure S3), and even previous work using Cu electrodes reported nearly double the hysteresis at  $4 \text{ mA/cm}^2$  (comparison is shown Figure S4).<sup>15</sup> To assist our understanding of the low hysteresis, electrochemical impedance spectroscopy was performed after initial plating cycles with  $0.25 \text{ mAh/cm}^2$  of fresh sodium (Figure 2b). We found the charge-transfer resistance, corresponding to the diameter of the semicircle in the Nyquist plot, to be extremely low and stable with cycling. Next, we performed plating/stripping testing at increased loadings of sodium (Figure 2c and Figure S5). We found that the electrodes exhibited stable performance at  $1 \text{ mA/cm}^2$  for 30 min plating times ( $0.5 \text{ mAh/cm}^2$ ) up to 8 h plating times ( $8 \text{ mAh/cm}^2$ ), with the Coulombic efficiency slightly increasing with loading, from 99.8% to 99.9%, indicating that the minor losses in the system occur during the initial seeding and/or the final stripping processes. To further demonstrate the versatility of this approach for exceptionally high loadings of sodium, 50 cycles were performed at  $12 \text{ mAh/cm}^2$  with the average Coulombic efficiency exceeding 99.9% (Figure 2d). These results are promising for the development electrodes with high aerial capacities, a focus of researchers who aim to minimize the cost of current collectors and separators.<sup>9,31,34</sup> To test the long-term durability, we ran over 1000 plating/ stripping cycles using 30 min plating times to maximize the initial seeding and final stripping events that appear most problematic (shown in Figure 2e). Nonetheless, we observed a highly stable hysteresis averaging 14 mV and a highly stable Coulombic efficiency averaging 99.8%, with no evidence of

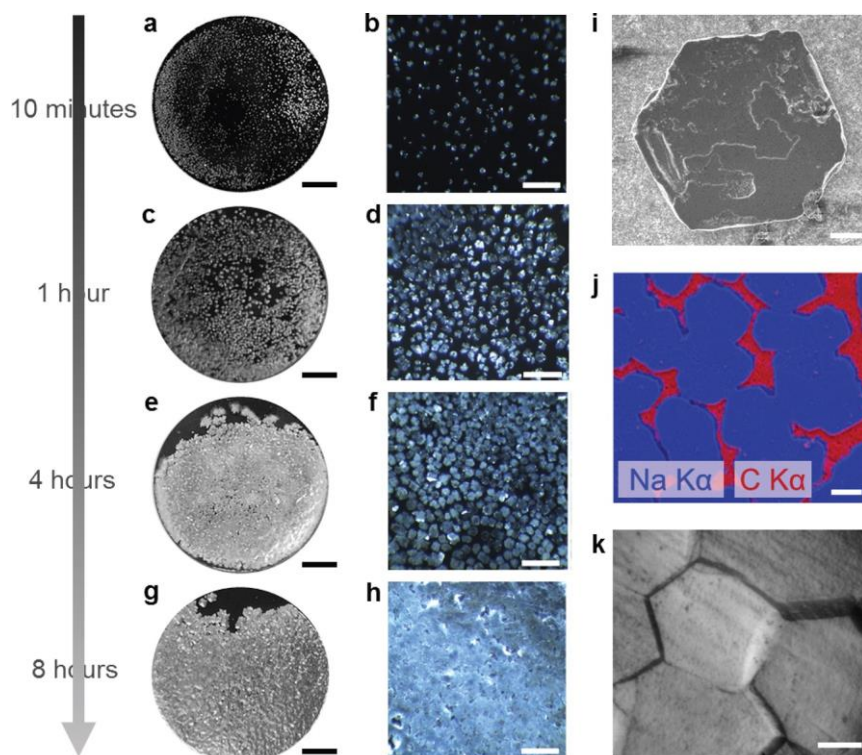


Figure 3. Photographs (SB = 2 mm) and micrographs (SB = 500 μm) of sodium metal on carbon/Al electrodes following plating at 0.5 mA/cm<sup>2</sup> for (a,b) 10 min, (c,d) 1 h, (e,f) 4 h, and (g,h) 8 h. (i) SEM image of hexagon-shaped sodium metal island (SB = 20 μm). (j) EDS map showing coalescing sodium metal islands (CB = 50 μm). (k) Micrograph of plated sodium metal film with 4 mAh/cm<sup>2</sup> loading (SB = 20 μm).

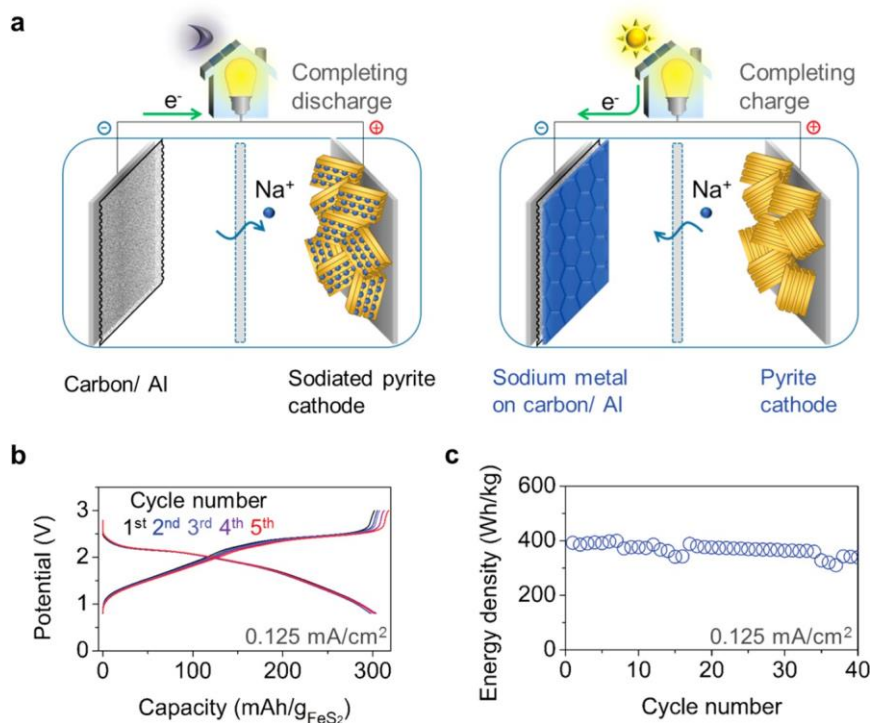


Figure 4. (a) Illustration of the charged and discharged states of the anode-free sodium battery utilizing the carbon/Al electrode. (b) Galvanostatic potential profiles of the full cell showing the first 5 cycles at 0.125 mA/cm<sup>2</sup> from 0.8 to 3.0 V with (c) the delivered energy density of the first 40 cycles with respect to the combined active mass of both electrodes.

short-circuiting or delaminating. Figure 2f shows the voltage profiles from the first, second, 499th, 500th, 999th, and 1000th cycles, which all appear nearly identical, emphasizing the stability maintained during cycling.

In order to gain insight into the plating process, carbon/Al electrodes were imaged with progressing sodium loading. Figure 3 shows electrodes after 10 min (a,b), 1 h (c,d), 4 h (e,f), and 8 h (g,h) of plating at 0.5 mA/cm<sup>2</sup>. From these images, we see a progression from the seeding of well-spaced islands of sodium to the growth and coalescence of these islands to form a smooth, shiny film of sodium metal. Interestingly, we found that the islands appear to grow as hexagons, as shown in the scanning electron micrograph (SEM) in Figure 3i, and the hexagonal pattern is maintained as the islands begin to coalesce together (shown in the energy dispersive X-ray spectroscopic map in Figure 3j) and persevered in the formed film, creating the appearance of polycrystallinity with defined grain boundaries (Figure 3k). To the best of our knowledge, this is the first documentation of such a plating process for alkali metals, which is especially interesting as it underlies extremely efficient and stable electrochemical performance. In comparison, the sodium film that is deposited on bare Al electrodes appears to exhibit a less defined pattern (Figure S6). It is also valuable to point out that, in good agreement with our previous testing, no evidence of dendritic growth was observed (Figure S7). Examining sodium plated at an increased current density of 4 mA/cm<sup>2</sup> (Figure S8), we observed smaller grains, supporting the recent work of Pei et al.,<sup>35</sup> but again found no presence of dendrites. We also note that our cross-sectional SEM images (Figure S9) appear to show that the sodium plating initially occurs above the carbon nucleation layer, which we attribute to the conductive nature of the carbon film and may be influenced by film properties such as morphology, pore size, etc.

Finally, to demonstrate the feasibility of using this plating approach for an anode-free cell configuration, we developed a full-cell anode-free sodium battery. To accomplish this, we employed pyrite (FeS<sub>2</sub>) for the cathode as it is a cheap, abundant material that has recently been shown to be an excellent candidate for SIBs with diglyme-based electrolytes.<sup>36</sup> However, since it natively does not contain sodium, we first presodiated the pyrite cathode prior to cell assembly, in a fashion similar to previous reports.<sup>37</sup> Full cells were constructed using presodiated pyrite paired with carbon/Al current collectors, corresponding to a discharged device state, as illustrated in Figure 4a. During the initial charge, the sodium ions are removed from pyrite during the oxidation reaction and reduced on the carbon/Al current collector to form sodium metal in situ. In this manner, we have developed a sodium metal battery that does not contain sodium metal on assembly. To prove that sodium metal was indeed forming during the charging process, we disassembled a fully charged full cell and show the plated sodium metal on the carbon/Al electrode in Figure S10. Initial voltage profiles exhibited during galvanostatic testing are shown with respect to the mass of the pyrite (assuming a Na<sub>1.5</sub>FeS<sub>2</sub> stoichiometry) in Figure 4b for the full cell following the initial charging process. Figure 4c shows the stability of the delivered energy density over 40 cycles with the corresponding capacity and Coulombic efficiency shown in Figure S11. The ~400 Wh/kg energy density, calculated based on the mass of the presodiated pyrite (assuming a Na<sub>1.5</sub>FeS<sub>2</sub> stoichiometry or a FeS<sub>2</sub> capacity of 335 mAh/g) and the carbon nucleation layer, exceeds all previous reports for SIBs and, assuming a 50% packaging penalty, exceeds current LIB technology. Going forward, better optimization of the cathode is expected to allow for increased cycling stability and improved rate capability.

In summary, we have demonstrated the use of a carbon nucleation layer to enable highly efficient and stable sodium plating and stripping as the basis for a new approach for sodium batteries: the anode-free sodium battery. The exceptional energy density of ~400 Wh/kg and versatility of this approach that builds upon naturally abundant low-cost materials and aqueous processing is the first demonstration that sodium batteries have the promise of outperforming LIB technology and filling the desperately needed demand for a cost-effective, highperformance battery for grid-scale storage.

## ASSOCIATED CONTENT

\* Supporting Information

The Supporting Information is available free of charge on the ACS Publications website at DOI: 10.1021/acs.nanolett.6b05174.

Details about electrochemical measurements, sodium imaging, cell assembly, Raman characterization of carbon nucleation layer, additional SEM and optical images of sodium depositions, half-cell cycling and rate performance, and full cell cycling performance (PDF)

## AUTHOR INFORMATION

ORCID

Saurav L. Chaudhari: [0000-0003-1191-9015](https://orcid.org/0000-0003-1191-9015) Ketan P. Pise: [0000-0003-3315-6960](https://orcid.org/0000-0003-3315-6960)

Notes

The authors declare no competing financial interest.

## REFERENCES

- (1) Larcher, D.; Tarascon, J. M. *Nat. Chem.* 2015, 7, 19–29.
- (2) Slater, M. D.; Kim, D.; Lee, E.; Johnson, C. S. *Adv. Funct. Mater.* 2013, 23, 947–958.
- (3) Li, H.; Peng, L.; Zhu, Y.; Chen, D.; Zhang, X.; Yu, G. *Energy Environ. Sci.* 2016, 9, 3399–3405.
- (4) Zhang, B.; Rousse, G.; Foix, D.; Dugas, R.; Corte, D. A. D.; Tarascon, J.-M. *Adv. Mater.* 2016, 28, 9824–9830.
- (5) Ding, J.; Zhou, H.; Zhang, H.; Stephenson, T. J.; Li, Z.; Karpuzov, D.; Mitlin, D. *Energy Environ. Sci.* 2017, 10, 153.
- (6) Peng, L. L.; Zhu, Y.; Chen, D. H.; Ruoff, R. S.; Yu, G. H. *Adv. Energy Mater.* 2016, 6, 1600025.
- (7) Stevens, D. A.; Dahn, J. R. *J. Electrochem. Soc.* 2000, 147, 1271–1273.
- (8) Lotfabad, E. M.; Ding, J.; Cui, K.; Kohandehghan, A.; Kalisvaart, W. P.; Hazelton, M.; Mitlin, D. *ACS Nano* 2014, 8, 7115–7129.
- (9) Shen, F.; Luo, W.; Dai, J. Q.; Yao, Y. G.; Zhu, M. W.; Hitz, E.; Tang, Y. F.; Chen, Y. F.; Sprenkle, V. L.; Li, X. L.; Hu, L. B. *Adv. Energy Mater.* 2016, 6, 1600377.
- (10) Bommier, C.; Surta, T. W.; Dolgos, M.; Ji, X. L. *Nano Lett.* 2015, 15, 5888–5892.
- (11) Zhu, H. L.; Jia, Z.; Chen, Y. C.; Weadock, N.; Wan, J. Y.; Vaaland, O.; Han, X. G.; Li, T.; Hu, L. B. *Nano Lett.* 2013, 13, 3093–3100.
- (12) Yu, X. W.; Manthiram, A. *Adv. Energy Mater.* 2015, 5, 1500350. (13) Hartmann, P.; Bender, C. L.; Vracar, M.; Dürer, A. K.; Garsuch, A.; Janek, J.; Adelhelm, P. *Nat. Mater.* 2013, 12, 228–232.
- (14) Iermakova, D. I.; Dugas, R.; Palacin, M. R.; Ponrouch, A. *J. Electrochem. Soc.* 2015, 162, A7060–A7066.
- (15) Seh, Z. W.; Sun, J.; Sun, Y.; Cui, Y. *ACS Cent. Sci.* 2015, 1, 449–455.
- (16) Cao, R.; Mishra, K.; Li, X.; Qian, J.; Engelhard, M. H.; Bowden, M. E.; Han, K. S.; Mueller, K. T.; Henderson, W. A.; Zhang, J.-G. *Nano Energy* 2016, 30, 825–830.
- (17) Luo, W.; Lin, C.-F.; Zhao, O.; Noked, M.; Zhang, Y.; Rubloff, G. W.; Hu, L. *Adv. Energy Mater.* 2016, 1601526.
- (18) Zheng, G. Y.; Lee, S. W.; Liang, Z.; Lee, H. W.; Yan, K.; Yao, H. B.; Wang, H. T.; Li, W. Y.; Chu, S.; Cui, Y. *Nat. Nanotechnol.* 2014, 9, 618–623.
- (19) Bai, P.; Li, J.; Brushett, F. R.; Bazant, M. Z. *Energy Environ. Sci.* 2016, 9, 3221–3229.
- (20) Kazyak, E.; Wood, K. N.; Dasgupta, N. P. *Chem. Mater.* 2015, 27, 6457–6462.
- (21) Wood, K. N.; Kazyak, E.; Chadwick, A. F.; Chen, K.-H.; Zhang, J.-G.; Thornton, K.; Dasgupta, N. P. *ACS Cent. Sci.* 2016, 2, 790–801. (22) Yang, C. P.; Yin, Y. X.; Zhang, S. F.; Li, N. W.; Guo, Y. G. *Nat. Commun.* 2015, 6, 8058.
- (23) Zhang, R.; Cheng, X. B.; Zhao, C. Z.; Peng, H. J.; Shi, J. L.; Huang, J. Q.; Wang, J. F.; Wei, F.; Zhang, Q. *Adv. Mater.* 2016, 28, 2155–2162.
- (24) Yun, Q. B.; He, Y. B.; Lv, W.; Zhao, Y.; Li, B. H.; Kang, F. Y.; Yang, Q. H. *Adv. Mater.* 2016, 28, 6932.
- (25) Liang, Z.; Zheng, G. Y.; Liu, C.; Liu, N.; Li, W. Y.; Yan, K.; Yao, H. B.; Hsu, P. C.; Chu, S.; Cui, Y. *Nano Lett.* 2015, 15, 2910–2916.
- (26) Yan, K.; Lu, Z.; Lee, H.-W.; Xiong, F.; Hsu, P.-C.; Li, Y.; Zhao, J.; Chu, S.; Cui, Y. *Nature Energy* 2016, 1, 16010.
- (27) Lin, D.; Liu, Y.; Liang, Z.; Lee, H.-W.; Sun, J.; Wang, H.; Yan, K.; Xie, J.; Cui, Y. *Nat. Nanotechnol.* 2016, 11, 626–632.
- (28) Xu, W.; Wang, J.; Ding, F.; Chen, X.; Nasybulin, E.; Zhang, Y.; Zhang, J.-G. *Energy Environ. Sci.* 2014, 7, 513–537.
- (29) Neudecker, B. J.; Dudney, N. J.; Bates, J. B. *J. Electrochem. Soc.* 2000, 147, 517–523.
- (30) Qian, J.; Adams, B. D.; Zheng, J.; Xu, W.; Henderson, W. A.; Wang, J.; Bowden, M. E.; Xu, S.; Hu, J.; Zhang, J.-G. *Adv. Funct. Mater.* 2016, 26, 7094–7102.
- (31) Wood, D. L.; Li, J. L.; Daniel, C. J. *Power Sources* 2015, 275, 234–242.

- (32) Cohn, A. P.; Share, K.; Carter, R.; Oakes, L.; Pint, C. L. *Nano Lett.* 2016, 16, 543–548.
- (33) Lu, L. L.; Ge, J.; Yang, J. N.; Chen, S. M.; Yao, H. B.; Zhou, F.; Yu, S. H. *Nano Lett.* 2016, 16, 4431–4437.
- (34) Bae, C. J.; Erdonmez, C. K.; Halloran, J. W.; Chiang, Y. M. *Adv. Mater.* 2013, 25, 1254–1258.
- (35) Pei, A.; Zheng, G.; Shi, F.; Li, Y.; Cui, Y. *Nano Lett.* 2017, DOI: [10.1021/acs.nanolett.6b04755](https://doi.org/10.1021/acs.nanolett.6b04755).
- (36) Hu, Z.; Zhu, Z. Q.; Cheng, F. Y.; Zhang, K.; Wang, J. B.; Chen, C. C.; Chen, J. *Energy Environ. Sci.* 2015, 8, 1309–1316.
- (37) Liu, N. A.; Hu, L. B.; McDowell, M. T.; Jackson, A.; Cui, Y. *ACS Nano* 2011, 5, 6487–6493.
- (38) Adam P. Cohn,<sup>†</sup> Nitin Muralidharan,<sup>‡</sup> Rachel Carter,<sup>†</sup> Keith Share,<sup>‡</sup> and Cary L. Pint\*,<sup>†,‡</sup> DOI: [10.1021/acs.nanolett.6b05174](https://doi.org/10.1021/acs.nanolett.6b05174)